Thermal-Structural Finite Element Analysis Using Linear Flux Formulation

Ajay K. Pandey*
Lockheed Engineering & Sciences Company, Hampton, Virginia 23666
and
Pramote Dechaumphai† and Allan R. Wieting‡
NASA Langley Research Center, Hampton, Virginia 23665

A linear flux approach is developed for a finite element thermal-structural analysis of steady-state thermal and structural problems. The element fluxes are assumed to vary linearly in the same form as the element unknown variables, and the finite element matrices are evaluated in closed form. Because numerical integration is avoided, significant computational time-saving is achieved. Solution accuracy and computational speed improvements are demonstrated by solving several two- and three-dimensional thermal-structural examples.

Nomenclature

A	= finite element area
$\{B\}$	= boundary load vector
c_{ij}	= material elastic constants
$[D_x], [D_y]$	= element matrices, Eq. (6)
E, F	= x and y flux components
H	= internal heat generation
h	= convective heat transfer coeff., Eq. (16); beam thickness, Eq. (30)
$[J]$	= Jacobian matrix
k	= thermal conductivity
ℓ	= beam length, Eq. (30)
ℓ, m, n	= components of unit normal vector
$[M]$	= mass matrix
$[N]$	= element interpolation function
$[P_x], [P_y]$	= element matrices, Eq. (11)
q	= heat flux
$\{R\}$	= load vector
s	= distance along boundary
T	= temperature
T_o	= reference temperature for zero stress
T_r	= fluid recovery temperature
T_s	= surface temperature
T_∞	= surrounding medium temperature
u, v, w	= displacement components
V_i	= element constants, Eqs. (21–28)
x, y, z	= coordinate directions
α	= coefficient of thermal expansion
ΔT	= temperature increment
ε	= emissivity, Eq. (16)
$\varepsilon_x, \varepsilon_y, \varepsilon_{xy}$	= strain components, Eq. (15)
σ	= Stefan-Boltzmann constant
$\sigma_x, \sigma_y, \tau_{xy}$	= stress components

Subscripts

s	= structural
T	= thermal

Superscripts

T	= transpose

*Principal Engineer. Member AIAA.
†Aerospace Technologist, Aerothermal Loads Branch. Member AIAA.
‡Head, Aerothermal Loads Branch. Member AIAA.

Introduction

FOR hypersonic vehicles to become a practical reality, efficient techniques are needed to analyze light-weight airframe and engine structures for repeated and prolonged exposure to their severe flight environment. To understand the structural response under these severe aerodynamic loads, research in the Aerothermal Loads Branch, NASA Langley Research Center has focused on developing effective computational approaches for predicting the aerodynamic flow and the thermal and structural response of the structure, including their interactions.[1] The approaches consist of using: 1) a general automated unstructured gridding to discretize the aerodynamic flowfield and the structure; 2) finite element methods to solve for the environment, loads, and response for all three disciplines (flow, thermal, and structural response); and 3) adaptive mesh refinement techniques with error indicators to minimize the number of grid points and increase the solution accuracy.

A Taylor-Galerkin finite element algorithm, has been used recently to predict the aerodynamic flowfield as well as the thermal-structural response for high-speed flow over leading edges.[2] The approach utilizes: 1) a Taylor series expansion in time to establish recurrence relations for time marching; and 2) the method of weighted residuals with Galerkin's criterion for spatial discretization. The governing equations are cast in conservation form. The standard primitive variables are replaced with their flux counterparts, which are assumed to vary linearly over the elements. This formulation allows the finite element matrices to be evaluated in closed form, thereby avoiding the more expensive numerical integration. Because the Taylor-Galerkin algorithm is a time-marching (transient) algorithm, the full benefits of the linear flux formulation for steady-state problems (steady-state heat transfer and static structural problems) has not been exploited. Furthermore, most structural problems may be treated as quasistatic even when the aerodynamic loads and the thermal response are transient.

The purpose of this paper is to extend the Taylor-Galerkin algorithm to steady-state thermal-structural analysis. The linear flux formulation and solution procedure are introduced. The finite element matrices (in integral forms), which are

different from those appearing in the conventional finite element formulation, are presented. A method to derive these finite element matrices in closed form is developed and presented for both two- and three-dimensional elements.

The capability of the linear flux formulation is demonstrated using four examples: 1) a thermal analysis of a circular plate with internal heat generation; 2) a structural analysis of a beam bending due to thermal load; 3) a thermal-structural analysis of a two-dimensional aerodynamically heated leading edge model; and 4) a structural analysis of a three-dimensional leading-edge model. Results are compared with available analytical solutions and the conventional finite element solutions.

Thermal-Structural Formulation

The derivation of finite element equations using a linear flux formulation is presented for steady-state thermal and structural analyses. For simplicity, the derivation presented herein is for two-dimensional problems. Extension to three-dimensional problems is straightforward. The governing equations are written in conservation form so that the linear flux formulation can be used directly. This formulation yields finite element matrices that can be evaluated in closed form. A method to evaluate these closed form matrices is described for both two- and three-dimensional elements.

Governing Equations

Heat Transfer

The steady-state thermal response of a structure is governed by the energy in conservation form

$$\frac{\partial}{\partial x}(E_T) + \frac{\partial}{\partial y}(F_T) = H_T \tag{1}$$

where the subscript T denotes the thermal analysis, E_T and F_T are the heat flux components, and H_T is the heat source per unit volume. The heat fluxes E_T and F_T are related to temperature gradients by Fourier's law.

Structural Response

The static structural response is governed by the equilibrium equations in conservation form

$$\frac{\partial}{\partial x}\{E_s\} + \frac{\partial}{\partial y}\{F_s\} = 0 \tag{2}$$

where the subscript s denotes the structural analysis. The vectors $\{E_s\}$ and $\{F_s\}$, which contain the stress components, are given by

$$\begin{aligned}
\{E_s\}^T &= [\sigma_x \quad \tau_{xy}] \\
\{F_s\}^T &= [\tau_{xy} \quad \sigma_y]
\end{aligned} \tag{3}$$

The stress components σ_x, σ_y, and τ_{xy} are related to the displacement gradients and the temperature by the generalized Hooke's law.

Solution Procedure

For simplicity in presenting the linear flux algorithm, both the steady-state energy equation and structural equilibrium equations are written in the form of a scalar equation as

$$\frac{\partial E}{\partial x} + \frac{\partial F}{\partial y} = H \tag{4}$$

Although the derivation presented below is for the thermal analysis, the procedure can be applied directly to the structural analysis.

Linear Flux Assumptions

The key feature of the linear flux formulation in the thermal analysis is to assume the distribution of the element heat fluxes E and F in the same form as the element temperature distribution T, that is

$$\begin{aligned}
T(x, y) &= [N(x, y)]\{T\} \\
E(x, y) &= [N(x, y)]\{E\} \\
F(x, y) &= [N)x, y)]\{F\}
\end{aligned} \tag{5}$$

where $[N(x, y)]$ are the element interpolation functions, and $\{T\}$, $\{E\}$ and $\{F\}$ are the vectors of the element nodal quantities. The assumption of a linear distribution of element fluxes E and F, which are interpolated in the same form as other dependent variables (e.g. T, as shown in Eq. (5)), is widely used in the computational fluid dynamics.[2]

Finite Element Equations

The finite element equations are derived using the method of weighted residuals.[3] The governing differential equation, Eq. (4), is multiplied by the weighting functions, $[N(x, y)]$, and integrated over the element area A. Integration by parts is performed to produce element integral terms and the boundary surface integral terms for application of different types of thermal boundary conditions. Details of the derivation follows the conventional finite element approach described in Ref. 3. The finite element equations obtained are in the form

$$[D_x]\{E\} + [D_y]\{F\} + \{R\} + \{B\} = 0 \tag{6}$$

In this equation, the matrices $[D_x]$ and $[D_y]$ are

$$[D_x] = \int_A \left\{\frac{\partial N}{\partial x}\right\} [N]\mathrm{d}\,A \tag{7a}$$

$$[D_y] = \int_A \left\{\frac{\partial N}{\partial y}\right\} [N]\mathrm{d}\,A \tag{7b}$$

The element nodal vector $\{R\}$ associated with the heat source H is defined as

$$\{R\} = \int_A \{N\}H\,\mathrm{d}\,A \tag{8}$$

The vector $\{B\}$ representing the boundary nodal vector is defined as

$$\begin{aligned}
\{B\} &= \int_s \{N\}[N]\mathrm{d}\,s(\ell\,\{E\} + m\{F\}) \\
&= \int_s \{N\}[N]\mathrm{d}\,s\{q\}
\end{aligned} \tag{9}$$

where ℓ and m are the components of a unit vector normal to the element boundary. The finite element matrices shown in Eqs. (7–9) are evaluated in closed form, as is demonstrated in the subsequent section.

Because the fluxes E and F are related to the temperature gradients given by Fourier's law

$$E = -k\frac{\partial T}{\partial x} \tag{10a}$$

$$F = -k\frac{\partial T}{\partial y} \tag{10b}$$

where k is the material thermal conductivity, the element nodal flux vectors, $\{E\}$ and $\{F\}$, can be expressed in terms of element nodal temperature $\{T\}$ as

$$\{E\} = -k[P_x]\{T\} \qquad (11a)$$

$$\{F\} = -k[P_y]\{T\} \qquad (11b)$$

where the matrices, $[P_x]$ and $[P_y]$, are related to the element shape and are given in the Appendix. The element nodal flux vectors, Eqs. (11a) and (11b), are substituted into Eq. (6) to obtain the final finite element equations in terms of the unknown element nodal temperature $\{T\}$ in the form

$$[K]\{T\} = \{R\} + \{B\} \qquad (12)$$

where the stiffness (or conduction) matrix, $[K]$, is given by

$$[K] = k[D_x][P_x] + k[D_y][P_y] \qquad (13)$$

Equation (12) is in a form similar to that obtained from the conventional finite element approach, except that the latter stiffness matrix is defined by

$$[\bar{K}] = \int_A k \left\{\frac{\partial N}{\partial x}\right\} \left[\frac{\partial N}{\partial x}\right] \mathrm{d}A + \int_A k \left\{\frac{\partial N}{\partial y}\right\} \left[\frac{\partial N}{\partial y}\right] \mathrm{d}A$$

$$(14)$$

Evaluation of the conventional stiffness matrix $[\bar{K}]$ for some element types, such as the two-dimensional quadrilateral and three-dimensional hexahedral elements, requires the use of numerical integration.

For nonlinear problems (e.g., due to temperature dependent thermal conductivity), Eq. (12) is solved by the Newton-Raphson iteration technique.[3,4] This procedure is identical to that used in the conventional finite element approach.

The approach presented for the thermal analysis is applied directly to derive the finite element equations for the structural analysis. The equations are identical to Eqs. (5–13), where the temperature vector $\{T\}$ is replaced by the displacement vector containing the components u and v in x and y directions, and the vectors $\{E\}$ and $\{F\}$ represent the element nodal stress components. For elastic isotropic materials, typical model stress components in two dimensions are obtained using the general constitutive relation given as

$$\begin{Bmatrix} \sigma_x \\ \sigma_y \\ \tau_{xy} \end{Bmatrix} = \begin{bmatrix} C_{11} & C_{12} & C_{13} \\ C_{12} & C_{22} & C_{23} \\ C_{13} & C_{23} & C_{33} \end{bmatrix} + (T - T_0) \begin{Bmatrix} \beta_x \\ \beta_y \\ 0 \end{Bmatrix} \qquad (15)$$

where C_{ij}, $i, j = 1, 2, 3$, are the material elastic constants; β_x and β_y are the thermal expansion parameters in the x and y directions, respectively. Explicit expressions of this Eq. (15) for two-dimensional plane stress and plane strain problems are given in Ref. 3.

Boundary Conditions

The boundary conditions for thermal analysis are applied via the boundary nodal vector $\{B\}$ shown in Eq. (9). The vector $\{q\}$ appearing in this equation may be replaced by different types of boundary conditions

$$q = \begin{cases} 0 & \text{(insulated)} \\ q_s & \text{(specified heating)} \\ h(T_s - T_r) & \text{(surface convection)} \\ \varepsilon\sigma(T_s^4 - T_\infty^4) & \text{(surface radiation)} \end{cases} \qquad (16)$$

The boundary conditions for the structural analysis, such as the applied surface pressure, can be added into the structural equations via the surface boundary vector. The procedure is identical to that for the thermal analysis previously described and is, therefore, omitted.

Derivation of Closed-Form Finite Element Matrices and Element Nodal Gradients

All finite element integrals, such as $[D_x]$, $[D_y]$, and $\{R\}$, which are given by Eqs. (7) and (8), can be expressed in closed forms. This is true for simple element types (rods, triangles, and tetrahedrons) as well as for more popular elements (quadrilaterals and hexahedrons). In addition, closed-form expressions for other finite element integrals (such as the consistent mass matrix) and the gradients of element variables (such as the consistent mass matrix) and the gradients of element variables (such as $\partial T/\partial x$), which are normally required in other finite element formulations, can be obtained by the procedure described below.

Quadrilateral Element

Typical finite element integrals for a general quadrilateral element, as shown in Fig. 1, are given below using natural coordinates:

$$[M] = \int_{-1}^{1} \int_{-1}^{1} [N]^T[N]|J| \, \mathrm{d}\xi \, \mathrm{d}\eta \qquad (17)$$

$$[D_x] = \int_{-1}^{1} \int_{-1}^{1} \left\{\frac{\partial N}{\partial x}\right\} [N]|J| \, \mathrm{d}\xi \, \mathrm{d}\eta \qquad (18)$$

where $[M]$ is the consistent mass matrix and $[D_x]$ is the element matrix previously defined in Eq. (7a). The determinant of the Jacobian $|J|$ represents the transformation from the element global $x - y$ coordinates to the natural coordinates $\xi - \eta$ (see Fig. 1). The transformation permits the element integration to be evaluated over a square. The determinant of the Jacobian for the two-dimensional quadrilateral element is

$$|J| = \begin{vmatrix} J_{11} & J_{12} \\ J_{21} & J_{22} \end{vmatrix}$$

$$= \begin{vmatrix} \dfrac{\partial}{\partial \xi} \sum_{i=1}^{4} (N_i x_i) & \dfrac{\partial}{\partial \xi} \sum_{i=1}^{4} (N_i y_i) \\ \dfrac{\partial}{\partial \eta} \sum_{i=1}^{4} (N_i x_i) & \dfrac{\partial}{\partial \eta} \sum_{i=1}^{4} (N_i y_i) \end{vmatrix}$$

$$= \frac{\partial}{\partial \xi} \sum_{i=1}^{4} (N_i x_i) \cdot \frac{\partial}{\partial \eta} \sum_{i=1}^{4} (N_i y_i)$$

$$- \frac{\partial}{\partial \xi} \sum_{i=1}^{4} (N_i y_i) \cdot \frac{\partial}{\partial \eta} \sum_{i=1}^{4} (N_i x_i)$$

$$(19)$$

where

$$N_i = N_i(\xi, \eta) = \tfrac{1}{4}(1 + \xi\xi_i)(1 + \eta\eta_i) \quad i = 1, \ldots, 4$$

$$(20)$$

The algebraic expression for the determinant of the Jacobian shown in Eq. (19) is in the form of the partial derivatives of the element interpolation functions $N_i(\xi, \eta)$ and the element nodal locations $(x_i, y_i; i = 1, \ldots, 4)$. The expression for the determinant of the Jacobian is quite lengthy (contains a total of 64 terms if fully expanded), and, thus, results in a tedious task for deriving the closed form element matrices [Eq. (17) and (18)]. Such a task becomes almost impossible for the three-dimensional eight-node hexahedral element in which the determinant of the Jacobian, if fully expanded, contains approximately 200,000 terms. To overcome this difficulty, the determinant of the Jacobian is rewritten in an alternate, simpler form

$$|J| = \sum \bar{N}_i(\xi, \eta) V_i \qquad (21)$$

where $\bar{N}_i(\xi, \eta)$ are the functions of the natural coordinates ξ and η, and are selected so that Eq. (21) represents the complete order of polynomials of ξ and η as appearing in the original Eq. (19). The unknown constants, V_i, are functions of the nodal coordinates and are to be determined. For a two-dimensional quadrilateral element, the functions, $\bar{N}_i(\xi, \eta)$, can be represented by the isoparametric quadrilateral element interpolation functions, $N_i(\xi, \eta)$, as given by Eq. (20). Equation (21) then becomes

$$|J| = \sum_{i=1}^{4} N_i(\xi, \eta)V_i$$
$$= N_1V_1 + N_2V_2 + N_3V_3 + N_4V_4 \qquad (22)$$

The unknowns V_i, $i = 1, \ldots, 4$ can then be determined easily using the properties of $N_i(\xi, \eta)$, that is $N_i(\xi, \eta)$ equal to unity at node i and zero at the other nodes. As an example, V_1 is obtained by equating Eqs. (22) and (19) with the property at node 1 ($\xi = \eta = -1$ in Fig. 1) to give

$$V_1 = [(x_2 - x_1)y_4 + (x_1 - x_4)y_2 + (x_4 - x_2)y_1]/4 \qquad (23)$$

The use of the determinant of the Jacobian in the form of Eq. (21) instead of the original Eq. (19) permits the finite element matrices [Eqs. (17) and (18)] to be evaluated in closed forms. The use of the symbolic manipulation program MACSYMA[5] greatly simplified this evaluation.

The determinant of the Jacobian in the form of Eq. (21) is also used to derive closed-form expressions for the element gradients. For example, the element temperature gradient, $\partial T/\partial x$, is given by

$$\frac{\partial T}{\partial x} = \frac{1}{|J|} \left(J_{22} \left[\frac{\partial N}{\partial \xi} \right] - J_{12} \left[\frac{\partial N}{\partial \eta} \right] \right) \{T\} \qquad (24)$$

where J_{12} and J_{22} are defined in Eq. (19). The temperature gradient at node 1 can be determined by setting $\xi = \eta = -1$ to yield

$$\frac{\partial T}{\partial x} \bigg|_{\text{node } 1} = \frac{(T_2 - T_1)y_4 + (T_1 - T_4)y_2 + (T_4 - T_2)y_1}{(x_2 - x_1)y_4 + (x_1 - x_4)y_2 + (x_4 - x_2)y_1} \qquad (25)$$

where subscripts denote the element node numbers shown in Fig. 1.

The approach presented here is used to derive closed form expressions for the other finite element matrices (e.g. $[D_y]$, and $\{R\}$) and nodal variable gradients. These closed-form expressions are used in the formulation for both thermal and structural analyses.

Hexahedral Element

The three-dimensional finite element matrices are in the same form as shown in Eqs. (17) and (18), except that integration is performed over the element volume. For an eight-
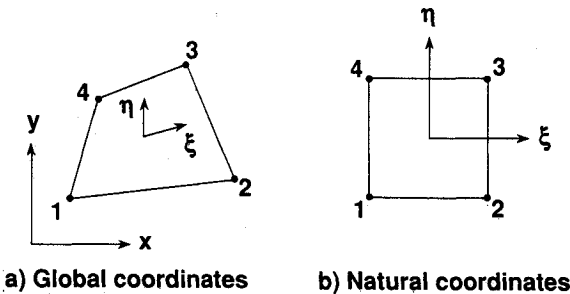

a) Global coordinates   b) Natural coordinates

Fig. 1 Quadrilateral finite element in two-dimensional global and natural coordinates.

a) Global coordinates   b) Natural coordinates
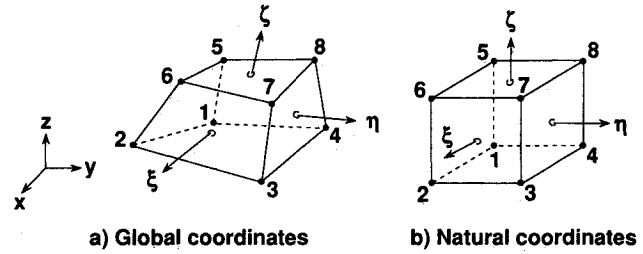
Fig. 2 Hexahedral finite element in three-dimensional global and natural coordinates.

node hexahedral element as shown in Fig. 2, the element interpolation functions are

$$N_i = N_i(\xi, \eta, \zeta) = \tfrac{1}{8}(1 + \xi\xi_i)(1 + \eta\eta_i)(1 + \zeta\zeta_i)$$
$$i = 1, \ldots, 8 \qquad (26)$$

and the determinant of the Jacobian is given by

$$|J| = \begin{vmatrix} \dfrac{\partial}{\partial \xi}(\Sigma N_i x_i) & \dfrac{\partial}{\partial \xi}(\Sigma N_i y_i) & \dfrac{\partial}{\partial \xi}(\Sigma N_i z_i) \\[2mm] \dfrac{\partial}{\partial \eta}(\Sigma N_i x_i) & \dfrac{\partial}{\partial \eta}(\Sigma N_i y_i) & \dfrac{\partial}{\partial \eta}(\Sigma N_i z_i) \\[2mm] \dfrac{\partial}{\partial \zeta}(\Sigma N_i x_i) & \dfrac{\partial}{\partial \zeta}(\Sigma N_i y_i) & \dfrac{\partial}{\partial \zeta}(\Sigma N_i z_i) \end{vmatrix} \qquad (27)$$

By following the procedure described in the previous section, the above determinant of the Jacobian is rewritten in an alternate simpler form as in Eq. (21). In three dimensions, the hexahedral element interpolation functions $N_i(\xi, \eta, \zeta)$, given in Eq. (26), cannot be used to represent the function, $\bar{N}(\xi, \eta, \zeta)$, in the same fashion as in the two-dimensional Jacobian formulation. This is because the hexahedral element interpolation functions, $N_i(\xi, \eta, \zeta)$, do not provide a complete polynomial as required by the determinant of the Jacobian shown in Eq. (27). Therefore the functions, $\bar{N}(\xi, \eta, \zeta)$, are represented by 27-node Langrange cubic element interpolation functions to obtain a simpler form for the Jacobian determinant, given as Eq. (28)

$$|J| = \sum_{i=1}^{27} N_i(\xi, \eta, \zeta)V_i \qquad i = 1, \ldots, 27 \qquad (28)$$

The unknowns V_i are determined by equating the Eqs. (27) and (28) at the nodal locations of the Lagrange cubic element. The program MACSYMA[5] was used to derive these unknowns V_i as well as the associated element matrices and the element nodal gradients in closed form. The algebraic expressions for the matrices and the gradients were very lengthy, therefore, they were translated into FORTRAN statements using MACSYMA and were used directly in the analysis code. The use of these closed-form expressions reduces the computational time compared to the traditional numerical integration, as is demonstrated in the next section.

Application

Four examples are presented to demonstrate the accuracy and computational efficiency of the linear flux formulation. These consist of: 1) a thermal analysis of a circular plate with internal heat generation; 2) a structural analysis of a beam bending due to thermal load; 3) a two-dimensional thermal-structural analysis of an aerodynamically heated leading-edge model; and 4) a three-dimensional structural analysis of an aerodynamically heated leading-edge model. Results obtained by the linear flux formulation are compared with available analytical solutions and the conventional finite element solutions.

Circular Plate with Internal Heat Generation

A 20 in. diam stainless steel circular plate with internal heat generation and specified zero temperature along the circumferential boundary shown in Fig. 3 is used as the first example. Analytical solution for the variation of temperature in the plate is available and is given by

$$T(r) = \frac{Q}{4k}(100 - r^2) \tag{29}$$

where Q is uniformly distributed internal heat generation rate per unit volume, k the plate thermal conductivity, and r the plate radial distance. Due to symmetry, only a quarter of the plate is modeled with 10 quadrilateral elements as shown in Fig. 3. The distorted quadrilateral element shape was selected to evaluate the formulation performance under an arbitrary unstructured mesh condition.

The plate temperature distribution obtained from the linear flux formulation is compared with the analytical solution [Eq. 29)] and the conventional finite element solution in Fig. 4. Because of the crude mesh used in the model, both finite element solutions underpredict the temperature distribution. The temperatures at nodes A, B, and C (see Fig. 3), obtained by the analytical method, linear flux approach, and the conventional approach are shown in Table 1. These results indicate that the linear flux formulation provides slightly higher solution accuracy compared to the conventional finite element formulation. This is due to the fact that four-Gauss-point numerical integration, which is commonly used to evaluate the conventional finite element stiffness matrix [see Eq. (14)], cannot provide exact integration for arbitrary quadrilateral element shapes.

The computational time for linear flux approach and the conventional approach are given in Table 2. The comparison of the computational time indicates a 39% savings for the linear flux approach. The time savings is due to the use of the closed-form algebraic expressions rather than the numerical integration to evaluate the finite element stiffness matrix.
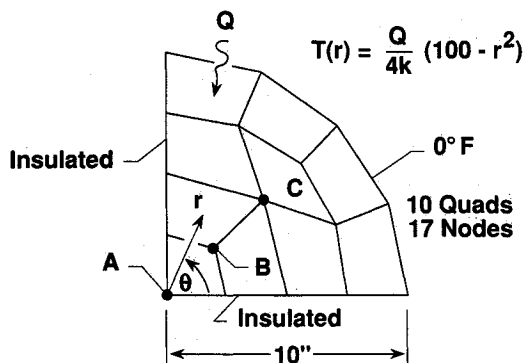

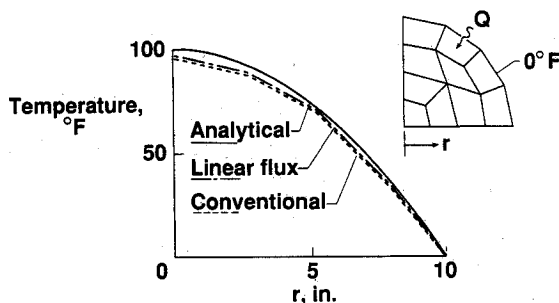Fig. 3 Finite element model for a 10-in.-radius circular plate subjected to internal heat generation.

Fig. 4 Comparative temperature distribution for 10-in.-radius circular plate subjected to internal heat generation.

Table 1 Comparative nodal temperature (°F) and errors

Location	Analytical Eq. (29)	Linear flux Temp.	Linear flux Error (%)	Conventional Temp.	Conventional Error (%)
A	100.0	96.9	3.1	96.5	3.5
B	92.0	88.3	4.0	87.9	4.4
C	68.0	67.8	0.3	67.3	1.0

Table 2 Comparative CPU time (CRAY-2 seconds) for evaluating element stiffness matrix

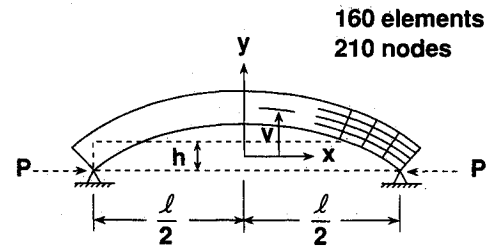| Linear flux	Conventional	% Saving
0.1036×10^{-3}	0.1690×10^{-3}	39

Fig. 5 A schematic finite element model of heated beam with boundary conditions.

Beam Bending Due to Thermal Load

As a second example, a 4 in. long, 0.1 in. thick stainless steel beam pinned on the bottom edges is considered and is shown in Fig. 5. The beam is assumed to be flat, and stress-free at room temperature. The beam temperature is raised uniformly by 65°F. The edge constraints cause the beam to bend into a convex shape. At this relatively low temperature and small deformation, beam structural response may be approximated by the beam-column theory,[6] in which shear effects are neglected. For cylindrical bending, flexural rigidity of the beam D is equal to $Eh^3/12$, where E is the modulus of elasticity and h is the thickness of the beam (see Fig. 5). The deflection $v(x)$ is given by[7]

$$v(x) = \frac{h}{2}\left(\frac{\cos \lambda x}{\cos \frac{\lambda \ell}{2}} - 1\right) \tag{30}$$

where ℓ is length of the beam and λ is $\sqrt{(P/D)}$. The axial constraint force P is computed from

$$\frac{P\ell}{hE} + \frac{h^2}{2}\lambda \tan\left(\frac{\lambda\ell}{2}\right)$$

$$+ \frac{h^2}{8}\frac{P}{D}\frac{\left(\frac{\ell}{2} - \frac{\sin \lambda\ell}{2\lambda}\right)}{\cos^2 \frac{\lambda\ell}{2}} - \alpha\Delta T\ell = 0 \tag{31}$$

where ΔT is the beam temperature increment.

Using symmetry, one-half of the beam is modeled with 160 quadrilateral finite elements. The finite elements are uniformly distributed with 40 elements along the beam length and 4 elements through the beam thickness. Both the linear flux and the conventional finite element approaches yield identical beam deflections. The predicted deflection distribution is compared with the solution from the beam theory, [Eq. (30)], in Fig. 6. The figure shows a very good agreement
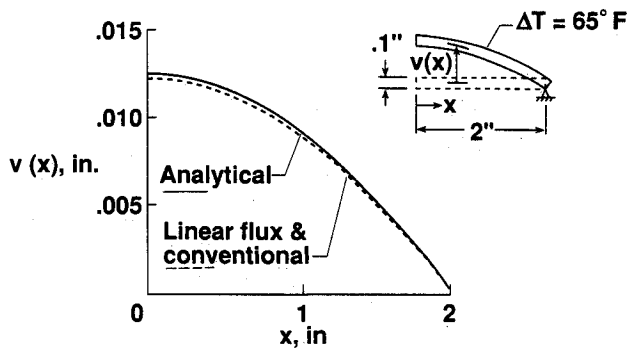
Fig. 6   Comparative deflections for a 4-in.-long beam subjected to uniform temperature increment of 65°F.
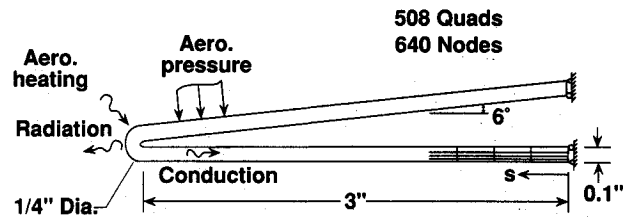

Fig. 7   A schematic thermal-structural finite element model of 0.25-in.-diam, 3-in.-long leading edge with boundary conditions.

of the beam deflection distributions with the maximum difference of about 2% at the beam center ($x = 0$).

The predicted beam deflection obtained from the linear flux formulation demonstrates the capability of the approach for providing the same solution accuracy as the conventional finite element approach for the structural analysis. Of course, the computational time saving of 39% is still achieved in the evaluation of the finite element stiffness matrix.

Two-Dimensional Leading Edge Model

To demonstrate further the capability of the linear flux formulation for both thermal and structural analyses, the approach is applied to predict the thermal-structural response of an aerodynamically heated leading edge subjected to a high-speed flow. The leading edge consists of a 0.25-in. nose diam, 3-in.-long model made of 0.1-in.-thick Inconel 617 alloy as shown in Fig. 7. The thermal boundary conditions along the outer surface consist of applied aerodynamic heating and emitted surface radiation. The leading edge is insulated along the inner surface. A schematic of the finite element model, which consisted of 508 quadrilateral elements is given in the figure. The mesh is graded with five elements through the thickness and 127 elements along the circumference. Approximately 70% of the elements lie in the 0.25-in. nose of the leading edge.

The aerodynamic heating along the leading-edge outer surface and the aerodynamic flowfield represented by the Mach number contours are shown in Fig. 8. These flow solutions were obtained from Ref. 8 by solving the Navier-Stokes equations. The Mach number contours indicate an unsymmetric bow shock shape from the freestream Mach 5.25 flow, which is inclined 12.5 deg relative to the bottom of the leading edge. The aerodynamic heating rate distribution is relatively low along both lower and upper surfaces of the leading edge compared to the stagnation point heating rate. The aerodynamic heating rate on the lower surface is slightly higher than the upper surface. The aerodynamic heating increases significantly at the nose because the flow stagnates in that region.

The leading-edge aerodynamic heating, shown in the Fig. 8, was predicted assuming a uniform surface temperature of 530°R. During the transient response, the aerodynamic heating rate decreases as the leading-edge temperature increases. Thus, to obtain a realistic leading-edge temperature response, the specified aerodynamic heating [q_s in Eq. (16)] is converted
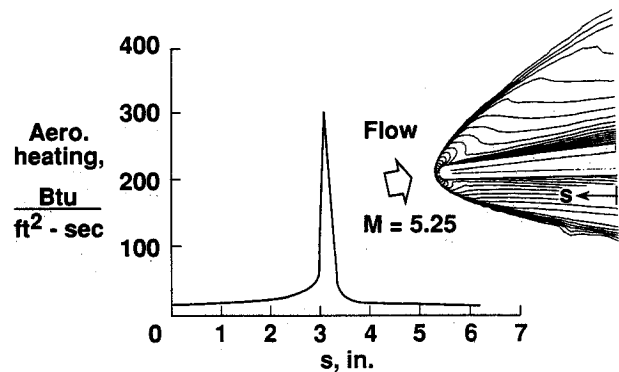

Fig. 8   Surface heating rate distribution and flow Mach number contours for an undisturbed Mach 5.25 flow over leading edge.
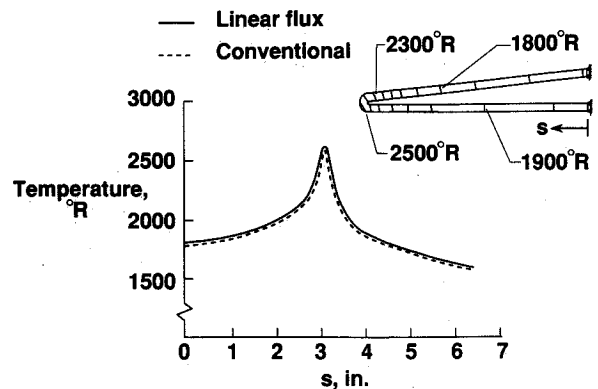

Fig. 9   Steady-state surface temperature distributions and leading-edge temperature contours.

into the surface convection boundary condition [$h(T_s - T_r)$ in Eq. (16)]. It should also be noted that the change in the surface convection coefficient h with the surface temperature T_s is small compared to the change in the heating rate q_s.

The predicted steady-state leading-edge temperature contours and the outer surface temperature distribution are compared with the conventional finite element solutions in Fig. 9. The temperature distributions obtained from both approaches are almost identical with the maximum difference of 0.2% at the nose of the leading edge where the peak temperature occurs.

The aerodynamic pressure on the leading edge and the flow pressure contours[8] are shown in Fig. 10. The peak pressure occurs at the flow stagnation point on the nose and the pressure is nearly uniform on the top and bottom surfaces. This aerodynamic pressure (Fig. 10) and the leading-edge temperature (Fig. 9) are used as the aerothermal loads for prediction of the leading-edge structural response. The leading-edge material properties, such as the modulus of elasticity and the coefficient of thermal expansion, are temperature-dependent.[9] The finite element discretization previously used in the thermal analysis is also used for the structural analysis to eliminate the data manipulation normally required by the different analysis disciplines. The predicted tangential stress contours superimposed on the deformed leading edge are shown in Fig. 11. The increased leading-edge temperature causes the leading edge to expand. The temperature difference between the lower and upper sections (higher temperature on the lower section) causes the leading edge to bend and rotate upward. The figure shows that the tangential stress, which is caused primarily by the temperature difference between the two sections, is relatively low. These results are in excellent agreement with the conventional finite element results indicating the validity of the linear flux formulation for the structural analysis. Again, a 39% computational time saving is achieved using the linear flux approach.

The predicted structural response obtained from the two-dimensional leading-edge model is based on a plane strain
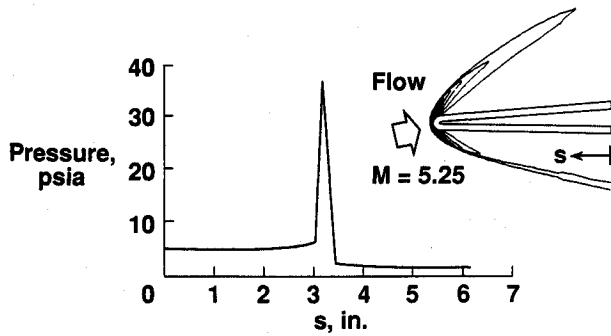
Fig. 10 Surface pressure distribution and flow pressure contours for an undisturbed Mach 5.25 flow over leading edge.
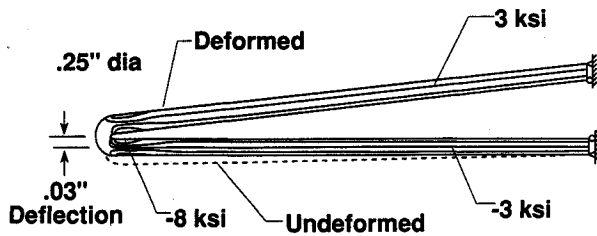

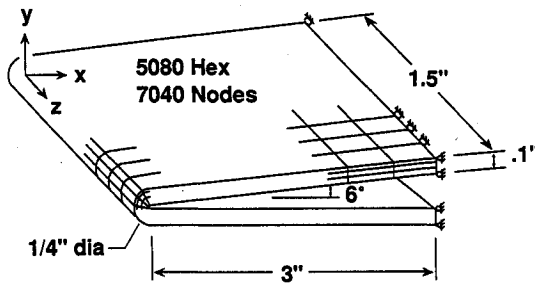**Fig. 11 Tangential stress contours on deformed leading edge.**

Fig. 12 A schematic three-dimensional finite element model of 0.25-in.-diam, 3-in.-long, 1.5-in.-wide leading edge with boundary conditions.
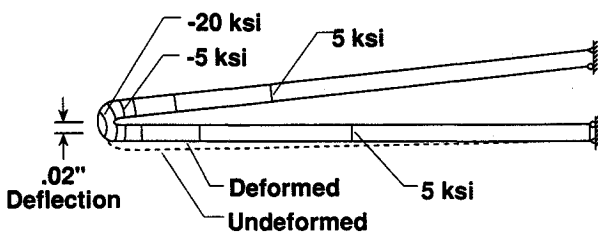

Fig. 13 Axial stress contours on deformed leading edge.

assumption. The use of this assumption results in high compressive axial stresses (≈ 150 ksi) in the direction normal to leading-edge cross section. A three-dimensional analysis with the appropriate boundary conditions would provide a more realistic leading-edge axial stress prediction. Such a structural analysis is presented in the next application.

Three-Dimensional Leading-Edge Model

As mentioned in the theoretical formulation section, the extension of the linear flux approach to three dimensions is straightforward. The approach has been extended for both the thermal and structural analyses using the eight-node hexahedral element. The use of the hexahedral element is preferred over other three-dimensional element types (such as the tetrahedral element) to reduce the computer memory required for the analysis (a hexahedral element consists of five

tetrahedral elements). The purposes of presenting this application is: 1) to compare the linear flux solution with the conventional finite element solution for a three-dimensional problem; 2) to demonstrate the computational time saving; and 3) to predict a more realistic leading-edge axial stress.

The linear flux approach is applied to predict the leading-edge structural response using the three-dimensional model shown in Fig. 12. The mesh on the leading-edge cross section (x-y plane) is identical to the two-dimensional model described in the previous example. The mesh is extended with a total of 10 layers in the z direction. The aerothermal loads consist of the temperature distribution (see Fig. 9) and the aerodynamic pressure (see Fig. 10), which are taken to be uniform in the z direction.

The predicted axial stress contours superimposed on the deformed leading edge along the midsection (section $z = 0.75$ in.) are shown in Fig. 13. This figure shows a more realistic axial stress distribution that resembles the temperature distribution. The peak compressive stress of approximately 20 ksi (compared to 150 ksi for 2-D model) occurs at the nose of the leading edge, where the temperature is maximum. This significant reduction occurs because there is no axial constraint as the two-dimensional case. The conventional finite element analysis solution is nearly identical with a maximum difference in the deflection at the leading-edge nose of less than 0.5%. The linear flux approach shows a computational time saving of 78% over the conventional finite element approach in the evaluation of the hexahedral element stiffness matrix. Such a significant computational time saving is due to the use of closed-form algebraic expressions instead of the eight-Gauss-point numerical integration. Of course, fewer Gauss-point integration could be used at the expense of accuracy.

Conclusions

A linear flux approach for finite element thermal-structural analysis was presented. The approach employs the assumption that the fluxes vary linearly as the dependent variables over the element. Such an assumption is widely used in computational fluid dynamics. The finite element equations for steady-state thermal and structural analyses are derived. The finite element equations consist of the finite element matrices in integral form that are different from those appearing in the conventional finite element formulation. A method was developed to derive these finite element matrices in closed form and the details of the derivation was described. The use of the closed-form algebraic expressions for evaluating the finite element matrices reduces the computational time by 39% for the 2-D problems and 78% for the 3-D problems compared to numerical integration. The linear flux formulation also yields slightly higher accurate results compared to the conventional finite element formulation.

Four thermal and structural problems were analyzed, and the results compare favorably with available analytical and conventional finite element results. The examples have demonstrated the viability of the approach to improve the disciplinary analysis efficiency for practical steady-state thermal-structural problems.

Appendix: Closed-Form Finite Element Matrices

The closed-form expressions of the finite element matrices for two-dimensional quadrilateral element, such as the $[D_x]$ matrix, shown in Eq. (7), are

$$D_x(1, 1) = -D_x(3, 3) = -(y_4 - y_2)/6$$

$$D_x(2, 2) = -D_x(4, 4) = -(y_1 - y_3)/6$$

$$D_x(1, 3) = -D_x(3, 1) = -(y_4 - y_2)/12$$

$$D_x(2, 4) = -D_x(4, 2) = -(y_1 - y_3)/12$$

$$D_x(1, 2) = -(y_4 + y_3 - 2 y_2)/12$$

$$D_x(1, 4) = -(2 y_4 - y_3 - y_2)/12$$

$$D_x(2, 1) = (y_4 + y_3 - 2 y_1)/12$$

$$D_x(2, 3) = -(y_4 - 2 y_3 + y_1)/12$$

$$D_x(3, 2) = (y_4 - 2 y_2 - y_1)/12$$

$$D_x(3, 4) = (2 y_4 - y_2 - y_1)/12$$

$$D_x(4, 1) = -(y_3 + y_2 - 2 y_1)/12$$

$$D_x(4, 3) = -(2 y_3 - y_2 - y_1)/12$$

where x_i and y_i, $i = 1, \ldots, 4$ are nodal coordinates of the element based on the element node numbering scheme shown in Fig. 1.

The element flux variation and the element nodal variables are related through the matrices $[P_x]$ and $[P_y]$ given in Eq. (11). The matrix $[P_x]$ as an example, is given by

$$P_x(1, 1) = (y_2 - y_4)/4 V_1$$

$$P_x(1, 2) = (y_4 - y_1)/4 V_1$$

$$P_x(1, 4) = (y_1 - y_2)/4 V_1$$

$$P_x(2, 1) = (y_2 - y_3)/4 V_2$$

$$P_x(2, 2) = (y_3 - y_1)/4 V_2$$

$$P_x(2, 3) = (y_1 - y_2)/4 V_2$$

$$P_x(3, 2) = (y_3 - y_4)/4 V_3$$

$$P_x(3, 3) = (y_4 - y_2)/4 V_3$$

$$P_x(3, 4) = (y_2 - y_3)/4 V_3$$

$$P_x(4, 1) = (y_3 - y_4)/4 V_4$$

$$P_x(4, 3) = (y_4 - y_1)/4 V_4$$

$$P_x(4, 4) = (y_1 - y_3)/4 V_4$$

$$P_x(1, 3) = P_x(2, 4) = P_x(3, 1) = P_x(4, 2) = 0$$

where V_i, $i = 1, \ldots, 4$ are the constants shown in Eq. (22), and are given by

$$V_1 = [(x_2 - x_1)y_4 + (x_1 - x_4)y_2 + (x_4 - x_2)y_1]/4$$

$$V_2 = [(x_2 - x_1)y_3 + (x_1 - x_3)y_2 + (x_3 - x_2)y_1]/4$$

$$V_3 = [(x_3 - x_2)y_4 + (x_2 - x_4)y_3 + (x_4 - x_3)y_2]/4$$

$$V_4 = [(x_3 - x_1)y_4 + (x_1 - x_4)y_3 + (x_4 - x_3)y_1]/4$$

References

[1]Wieting, A. R., Dechaumphai, P., Bey, K. S., Thornton, E. A., and Morgan, K., "Application of Integrated Fluid-Thermal-Structural Analysis Method," Presented at the Sixteenth Congress of the International Council of the Aeronautical Sciences, Jerusalem, Israel, Aug. 28–Sept. 2, 1988.

[2]Dechaumphai, P., Thornton, E. A., and Wieting, A. R., "Flow-Thermal-Structural Study of Aerodynamically Heated Leading Edges," AIAA Paper 88-2245-CP, April 1988.

[3]Huebner, K. H., and Thornton, E. A., *The Finite Element Method for Engineers*, Wiley, New York 1982.

[4]Bathe, K. J., *Finite Element Procedures in Engineering Analysis*, Prentice-Hall, Englewood Cliffs, NJ, 1982.

[5]The Mathlab Group, *MACSYMA Reference Manual*, The Mathlab Group Laboratory for Computer Science, MIT, Version 9, 2nd printing, Dec. 1977.

[6]Boley, B. A., and Weiner, J. H., *Theory of Thermal Stresses*, Wiley, New York, 1960.

[7]Thornton, E. A., and Dechaumphai, P., "Coupled Flow, Thermal, and Structural Analysis of Aerodynamically Heated Panels," *Journal of Aircraft*, Vol. 25, No. 11, Nov. 1988, pp. 1052–1059.

[8]Dechaumphai, P., Wieting, A. R., and Pandey, A. K., "Flow-Thermal-Structural Interaction of Aerodynamically Heated Leading Edges," AIAA Paper 89-1227-CP, April 1989.

[9]Metals Handbook Committee, *Metals Handbook*, 8th ed., American Society for Metals, OH, 1975.